Reprinted from THE ASTROPHYSICAL JOURNAL
Vol. 140, No. 1, July 1, 1964

14p

ON THE INFLUENCE OF THE CHEMICAL COMPOSITION ON THE STRUCTURE AND METAL INDEX OF STELLAR ATMOSPHERES*

DAVID FISCHEL
Goethe Link Observatory, Indiana University; and Ames Research Center, NASA, Moffett Field, California
Received December 20, 1963; revised March 6, 1964

ABSTRACT

A series of model stellar atmospheres, representing stars of normal and low heavy-element abundance in the spectral range F0–K0, have been calculated. Characteristics of the emergent flux of the models, particularly the metal index and (v, b, y)-colors of Strömgren's narrow-band photometric system, are discussed and compared with observations.

I. INTRODUCTION

The purpose of this investigation was to attempt to calibrate the metal index of Strömgren's (1958) scheme of narrow-band photometry. The metal index, m_1, is defined by three narrow-band filters, centered at 4100 Å, 4700 Å, and 5500 Å, respectively, and having half-widths of about 100 Å. If the magnitudes of a star observed through these three filters are designated as v, b, y, respectively, the metal index is

$$m_1 = (v - b) - (b - y) + \text{const} . \quad (1)$$

Thus, m_1 is in the form of a color index which measures the amount of energy absorbed in the v region, relative to the comparatively line-free y region of the spectrum (Strömgren 1963).

To carry out this calibration, the following procedure was adopted. Six sets of model atmospheres were constructed, each set characterized by a value of the total emergent flux, as tabulated by Allen (1955), for main-sequence stars of spectral types F0, F5, G0, G2, G5, and K0, with effective temperatures of 7500°, 6470°, 6000°, 5785°, 5360°, and 4910° K, respectively. Each set is composed of four models differing only in the value of the hydrogen-to-metal ratio, A, by number of atoms. These values are 1.9×10^4 (the normal main-sequence value) and 3, 10, and 100 times this value corresponding to $\frac{1}{3}$, $\frac{1}{10}$, and $\frac{1}{100}$ depletion of the abundance of the metals, respectively. Thus the known range of metal abundance differences for solar-type stars was roughly covered. No account was taken of abundance differences among the metals with changing hydrogen-to-metal ratio, as detected by such investigators as Wallerstein and Carlson (1960). Table 1 gives the parameters used in the calculation. Columns one and four refer to normal main-sequence stars; this use of spectral type is not customary.

II. THE MODEL ATMOSPHERES

All the models were calculated assuming the fractional abundance of hydrogen by mass, X, to be 0.8 and a helium-hydrogen ratio by number of 0.0625. In the radiative regions, the temperature distribution was adjusted by the method of Swihart (1956). In the convective regions, Vitense's (1953) procedure was adopted. The contribution of the metals to the electron pressure was explicitly included.

The continuous absorptions due to the hydrogen atom, the negative hydrogen ion, and Rayleigh scattering by hydrogen atoms were accounted for in the calculation. The

* Based on a thesis submitted in partial fulfilment of the Ph.D. degree in the Astronomy Department of Indiana University. *Publications of the Goethe Link Observatory, Indiana University*, No. 60.

cross-sections for H^- were taken from Geltman (1962) for the bound-free transitions and from T. and H. Ohmura (1961) for the free-free transitions.

A model solar atmosphere calculated using the above-mentioned sources of continuous opacity fits the observed flux distribution in the infrared (Johnson 1950). The observational data are flux-averaged over 100 Å regions. In the infrared region, to the redward of 10000 Å, there are very few absorption lines and, in any case, little energy is lost to them; so the observations represent the true amount of energy in the continuum at those wavelengths.

To the blueward of 10000 Å there is a considerably larger number of absorption lines, which absorb a significant amount of energy. In the case of the Sun, if all the absorption lines were filled in with radiation, the total surface flux would be 10 per cent greater. The fourth column in Table 1 gives estimates of this quantity for the six spectral types considered here.

In this work the effects of lines were included in two ways. For calculating the temperature-pressure relation of the model atmosphere, two line terms were added to the continuous absorption: (1) a semiempirical expression was used to account for the effect

TABLE 1

MODEL PARAMETERS

Spectral Type	F_{total} (erg $cm^{-2}sec^{-1}$)	$\log_{10} g$ (cm sec^{-2})	$\delta F/F$ (Per Cent)*
F0.....	1.794×10^{11}	4.3	5
F5.....	9.935×10^{10}	4.4	6.5
G0.....	7.348×10^{10}	4.4	10
G2.....	6.352×10^{10}	4.4	10
G5.....	4.680×10^{10}	4.4	15
K0.....	3.295×10^{10}	4.5	25:

* This column represents the increase in emergent flux if the absorption lines are filled in with radiation (Melbourne 1960; Allen 1955). The colon indicates that the number is very uncertain.

of the many weak lines which depress the continuum but do not appear as individual lines on spectrograms; (2) the effect of discernible absorption lines was included by a rough method based on Labs's (1951) statistics.

These two terms account for the effects of "blanketing" and "blocking" as discussed by Wildey, Burbidge, Sandage, and Burbidge (1962). See the Appendix for the forms used.

In the second phase of this investigation, the temperature-pressure relation obtained in the first phase was used to compute the emergent fluxes in individual lines. In that part of the work, only the first of the above terms was included and the second was replaced by individual line-absorption coefficients.

III. THE ABSORPTION LINES

The temperature-pressure relations thus obtained were then used to compute the emergent flux, point by point, across the wavelength regions of the (v, b, y)-filters, including explicit calculations of strong lines and blends as well as the continuum between lines. These results were multiplied by the transmission of the filters and integrated to obtain theoretical (v, b, y)-magnitudes and m_1's.

The emergent flux at a frequency, ν, is

$$F_\nu(0) = 2\pi\int_0^\infty E_2(t_\nu)B_\nu(t_\nu)\,dt_\nu, \qquad (2)$$

where $B_\nu(t_\nu)$ is the Planck function and t_ν is the total optical depth including all sources of opacity.

Of the lines which have central wavelengths lying in the three filter regions, 1560 were considered. These lines were chosen on the basis of the abundance of the element to which they belong, their gf-value, and lastly, their excitation potentials, X_{ex}. The abundances tabulated by Goldberg, Müller, and Aller (1960) were used. For elements not investigated by them, reference was made to Aller (1961). The gf-values and excitation potentials were taken from Corliss, Meggers, and Bozman (1962) for metal lines. Data for non-metal lines were taken from Moore (1945), Jurgens (1954), Kingsbury (1955), and Ornstein and Key (1934). Partition functions were taken from Claas (1951).

The selection of the absorption lines occurring in the three filter regions requires some criterion to prevent their number from becoming too large. With A_{el} defined as the ratio of the number of atoms of the element to the number of hydrogen atoms, the criterion

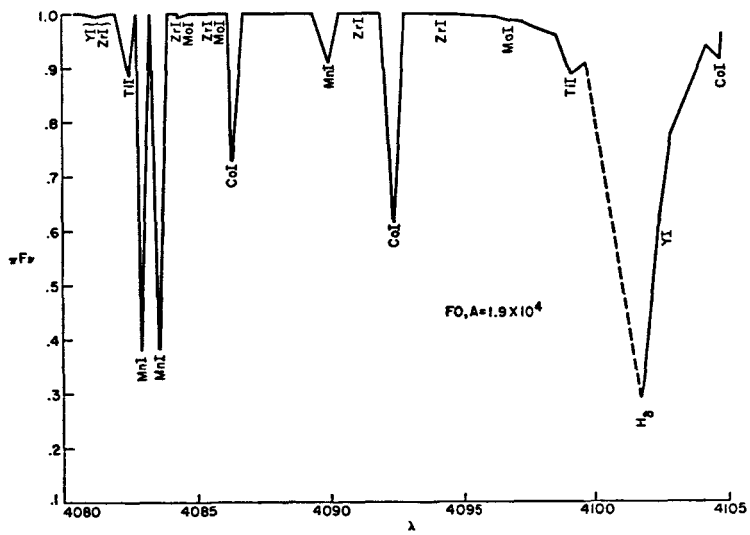

FIG. 1.—Triangular line profiles for F0, $A = 1.9 \times 10^4$ model from 4080 Å to 4105 Å

was adopted that A_{el} gf exp $(-X_{ex}/kT_m) > 10^{-8}$, where gf ≥ 1 and T_m was a large temperature, about 20000° K. There were 1500 lines selected in this manner.

In portions of the spectrum where the lines are widely separated, individual lines are replaced by triangles (see Figs. 1–3). First, the emergent flux at the center of the line is computed accounting for the depth-dependent line-absorption coefficient. It is then assumed that the line extends for an interval $|\Delta\lambda|$ to either side of the center, given by

$$\Delta\lambda = \Delta\lambda_D\left[1 + \frac{F_1}{F_{cont}}(35 + 10\log_{10} a)\right], \tag{3}$$

where F_1/F_{cont} is the fractional depression of the center of the line. The Doppler width, $\Delta\lambda_D$, and the damping parameter, a, are calculated at a depth with temperature near the effective temperature. Equation (3) was arrived at by graphing the results of Wrubel's (1962) investigation of the line profiles in Milne-Eddington type atmospheres. At the points $\lambda \pm \Delta\lambda$ it is assumed the continuum was reached and the continuous flux was computed.

If the lines were so close together that the centers of adjacent lines are closer than

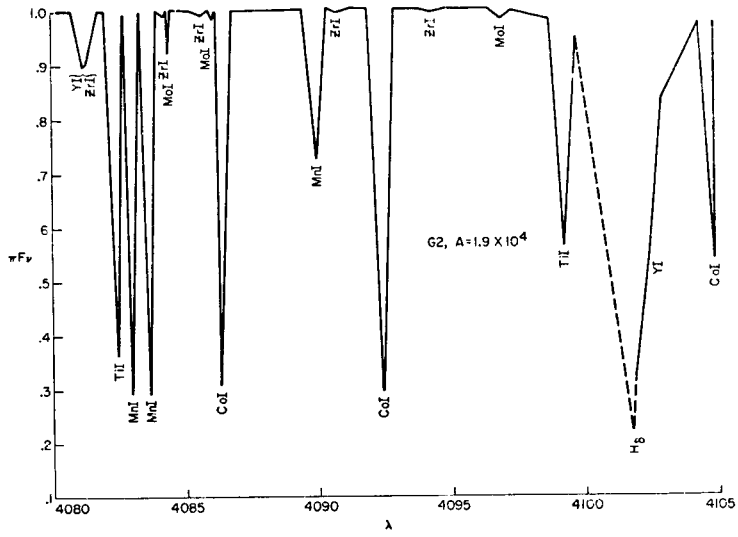

FIG. 2.—Triangular line profiles for G2, $A = 1.9 \times 10^4$ model (Sun) from 4080 Å to 4105 Å

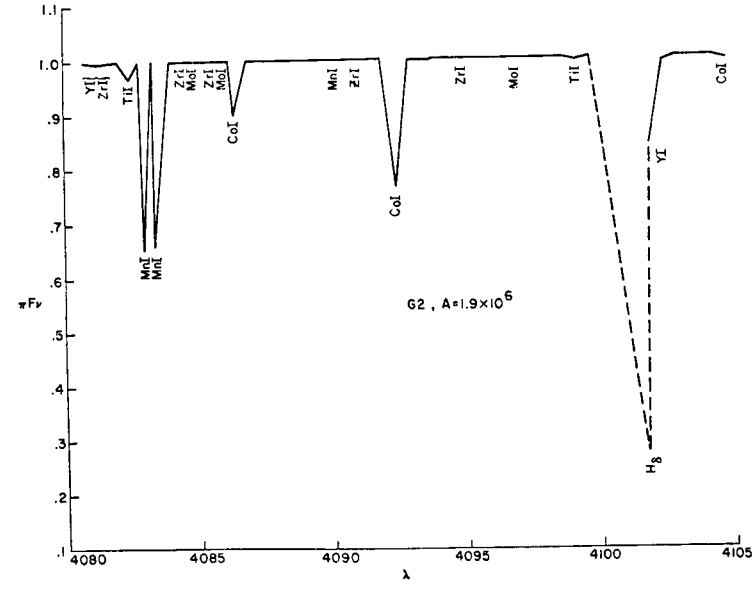

FIG. 3.—Triangular line profiles for G2, $A = 1.9 \times 10^6$ model (extreme subdwarf) from 4080 Å to 4105 Å.

0.5 Å, another procedure was used. First, contributions from the wings of neighboring lines were added when computing the absorption coefficient at the center of the principal line. Second, instead of using $\Delta\lambda$ of equation (3), the emergent flux is calculated at the wavelength midway between the centers of the adjacent lines and includes contributions to the absorption coefficient from all lines within 0.5 Å.

An exception to this last technique was made when the wavelength point under consideration occurred near an exceptionally strong line, such as the H- and K-lines of Ca II or the Balmer lines. Griem's (1960) theory was used for the absorption coefficient for the Balmer lines. Therefore, when the wavelength point is within 20 Å of the centers of these strong lines, the contributions from the wings of their absorption coefficient were added to the absorption coefficient.

Finally, the intensity as would be seen through a filter is calculated from

$$\langle F_\lambda \rangle = \int_{\lambda_1}^{\lambda_2} S_\lambda F_\lambda \, d\lambda \,, \tag{4}$$

where S_λ is the transmission coefficient at the wavelength λ. Expressing $\langle F_\lambda \rangle$ in magnitude units yields the magnitude at that filter region.

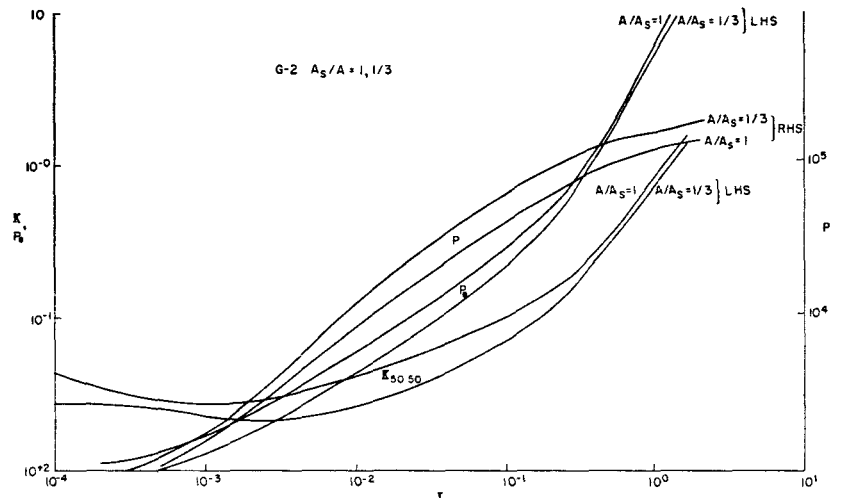

FIG. 4.—Pressure, electron pressure, and opacity as a function of the standard optical depth for the two G2 models of $A = 1.9 \times 10^4$ and 5.7×10^4.

IV. DISCUSSION OF RESULTS

a) Discussion of the Models

With the exception of the four K0 models and the G5 models with $A = 1.9 \times 10^4$ and 5.7×10^4 (Fischel 1963), which are discussed below, the temperature, electron pressure, and opacity decrease and the gas pressure increases as A increases (Przybylski 1961). Figure 4 demonstrates this for two G2 models. This follows very simply from a consideration of the normal equations for the stellar atmosphere. The opacity, primarily due to H^-, is proportional to the electron pressure, P_e, which is very nearly equal to P_g/A, where P_g is the gas pressure. The equation of hydrostatic equilibrium,

$$\frac{dP_g}{d\tau} = \frac{g}{\kappa} \,, \tag{5}$$

where κ is the opacity, g the acceleration due to gravity, and τ the optical depth, tells us then that $P_g \sim A^{1/2}$. It then follows that P_e and the opacity are proportional to $A^{-1/2}$. The temperature decreases as A increases because of the decreased effect of blanketing and blocking. The decreased temperature and the decreased absorption, particularly in the infrared, where the only absorption is due to H^-, caused by the increase in A, enhance the infrared region of the spectrum (see Fig. 5). The Balmer discontinuity is enhanced as A increases as a result of a decrease in blanketing and H^- absorption, both of which are proportional to P_e or, equivalently, to $A^{-1/2}$ (Strömgren 1940).

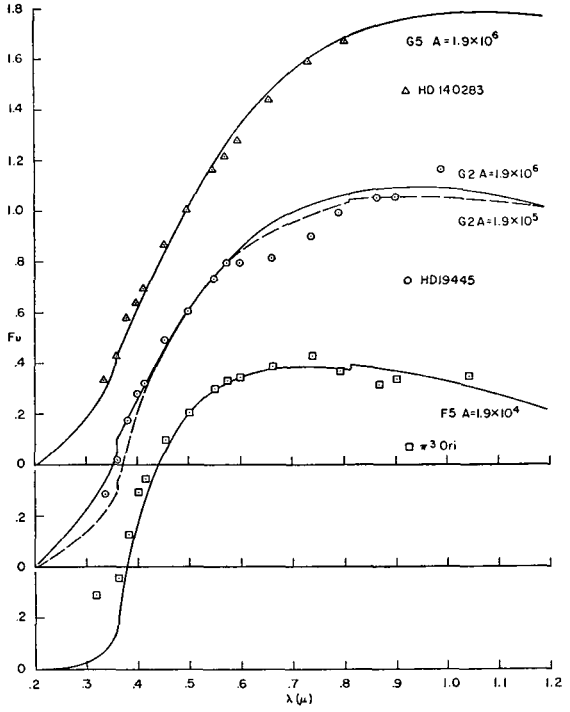

FIG. 5.—Emergent monochromatic flux (normalized to the flux at 5050 Å) as a function of λ for F5, $A = 1.9 \times 10^4$ (*lower solid curve*); G2, $A = 1.9 \times 10^5$ (*dashed curve*); G2, $A = 1.9 \times 10^6$ (*middle solid curve*) and G5, $A = 1.9 \times 10^6$ (*upper solid curve*) as compared with the observations of π^3 Orionis (*squares*), HD 19445 (*circles*), and HD 140283 (*triangles*). Note shifting ordinate axis.

The K0 models and the two G5 models mentioned above are poorly determined because of the severe blanketing that occurs in these stars. As noted below, these models give unrealistic values of m_1 and $b - y$. The method described in Section II is woefully inadequate for such strongly blanketed stars. Furthermore, molecules have been neglected in the calculations. The effect of molecules is probably more important for the T-P distribution and blanketing and the resultant radiation field, than for the specific wavelength regions of the (v, b, y)-filters. The filters cover such a small wavelength region that only the exclusion of many weak lines or a few very strong lines will affect the color for the models considered here.

Furthermore, this method is also inadequate for hotter stars which have a respectable number of saturated lines, as demonstrated by the normal G2 model (Sun) for which the

region near the Balmer discontinuity is excessively depressed relative to the observations of Johnson (1950) (see Fig. 6).

The models from G2 and F0 demonstrate the enhancement of the ultraviolet and blue regions of the spectrum due to decreased blanketing and a slight enhancement of the infrared due to decreased H^- absorption as A increases. Comparison with the observations of π^3 Orionis, HD 140283 and HD 19445 by Melbourne (1960) and Code (1959) shown in Figure 5 shows that the models are fair representations of real stars. The comparison is somewhat better than that of earlier work by Swihart and Fischel (1961). They used the H^- free-free transition probabilities of Chandrasekhar and Breen (1945) which are about twice those of T. and H. Ohmura (1961). Melbourne associates with π^3 Orionis (F6 V) an effective temperature of 6750° K. The model, an F5 V, is somewhat cooler, 6470°. A slightly hotter model should improve the fit. The fit to HD 19445 by Melbourne is 5800°, and the models in Figure 5 are 5785° K. Wallerstein (1962) has determined that the metals are underabundant by a factor of 56. The two sdG2 models represent atmospheres with factors 10 and 100, respectively, in the metal depletion. The

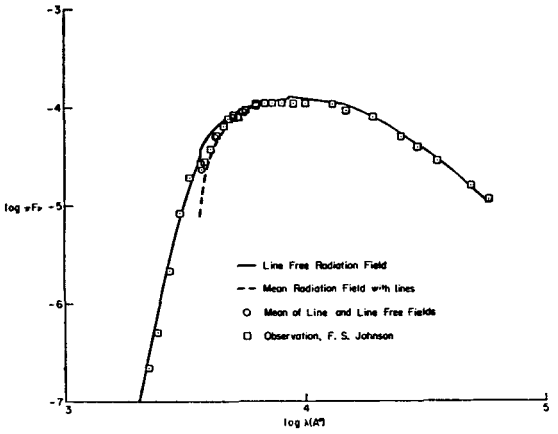

FIG. 6.—The decadic logarithm of the emergent monochromatic flux of the solar model (G2, $A = 1.9 \times 10^4$) as compared with the observational data for the Sun (*squares*), as functions of the decadic logarithm of the wavelength in Ångstroms.

problem in fitting theoretical calculations to these observations of HD 19445 lies in the depression of the observed points between 0.6 μ and 0.8 μ. A sdG0 model minimizes the deviation of the observations from the calculations in this region, but then the points redward of 0.8 μ are significantly more intense than the model. The fit to HD 140283 seems to be very fine, considering this model with an effective temperature of 5360° K to be slightly cooler than the estimated effective temperature of 5450° by Melbourne. Baskek (1959) estimates that $T_e = 5940°$, but a model of $T_e = 6000°$ K is not red enough to fit the observations.

Figure 7 demonstrates that subdwarfs are cooler than their corresponding main-sequence types and are therefore redder, as described above. The figure also shows that the convection zone (1) begins closer to the surface in optical depth, as A increases, (2) begins deeper in linear distance as A increases, and (3) begins nearer the surface as the total emergent flux increases.

The latter three effects can be seen to follow from considerations of the logarithmic temperature-pressure gradient and the definition of optical depth. Writing

$$\nabla \sim \kappa P T^{-4} \tag{6}$$

for the radiative region (Vitense 1953) and using the above dependence of κ and P on A, we have

$$\nabla \sim A^{-1/2} A^{1/2} T^{-4} \sim T^{-4} . \tag{7}$$

Now

$$\frac{d\nabla}{dA} \sim -4T^{-5} \frac{dT}{dA} , \tag{8}$$

and since

$$\frac{dT}{dA} < 0 , \tag{9}$$

we have that

$$\frac{d\nabla}{dA} > 0 . \tag{10}$$

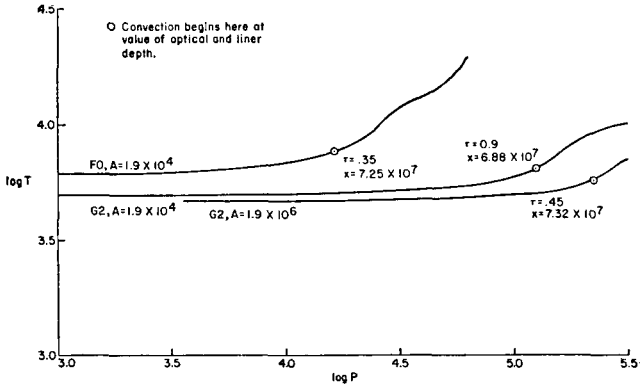

FIG. 7.—Temperature as a function of pressure for the models F0, $A = 1.9 \times 10^4$ (*upper curve*), G2 (Sun), $A = 1.9 \times 10^4$ (*middle curve*), and G2, $A = 1.9 \times 10^6$, an extreme subdwarf (*lower curve*). The portion of each curve to the left of the circle lies in the radiative equilibrium region. That to the right lies in the convecting region.

This may be interpreted that ∇ becomes superadiabatic at smaller values of τ as A increases, confirming result (1).

The definition of optical depth, measuring x downward, is

$$\tau \sim \kappa \rho x . \tag{11}$$

From the above relations, we have $d\kappa/dA \sim -A^{-3/2}$ and $d\rho/dA \sim A^{1/2}$. We assert that with increasing A, κ decreases faster than ρ increases. Therefore, an increase in A requires a longer linear distance in order to accumulate the same optical distance as the model with the normal value of A. Since result (1) yields $d\tau_c/dA < 0$, κ decreases fast enough that

$$\frac{dx_c}{dA} > 0 , \tag{12}$$

where τ_c and x_c are the optical and linear distances to the beginning of the convection zone.

As the total emergent flux increases, the degree of ionization of hydrogen increases and the adiabatic temperature gradient decreases. This permits convection to commence at a shallower optical and linear depth, that is, result (3).

b) Discussion of the Metal Indices

Figures 1–3 demonstrate the result of having two methods for calculating the wings of lines. If one side of the profile was calculated using equation (3) and the other side taken as halfway to the next line center, the result often is an artificially asymmetric line. Since $\Delta\lambda$ of equation (3) seems to be too large, this effectively removes extra energy from the spectrum. Examples are the Zr I lines near 4085 Å. Since too few lines were considered, as discussed below, this error compensates slightly for the insufficient amount of data. The profiles of Hδ are dotted in, with points taken from Aller and Greenstein (1960), because Hδ has no central component (gf = 0) and was initially deleted from the list of central wavelengths, although its wings were accounted for, according to the criterion of Section III. The calculations for m_1 did include it in the list of wavelengths.

Since we do not have a general theory of microturbulence for stellar atmospheres, the microturbulent velocity was neglected in the calculation of the Doppler width. Wallerstein (1962) notes that the turbulent velocity decreases with decreasing metal abundance. The models do not show any such effect in their convection zones. (This is because of the inadequacy of methods for handling convection in models.) Including a microturbulence field should improve the main-sequence calculations.

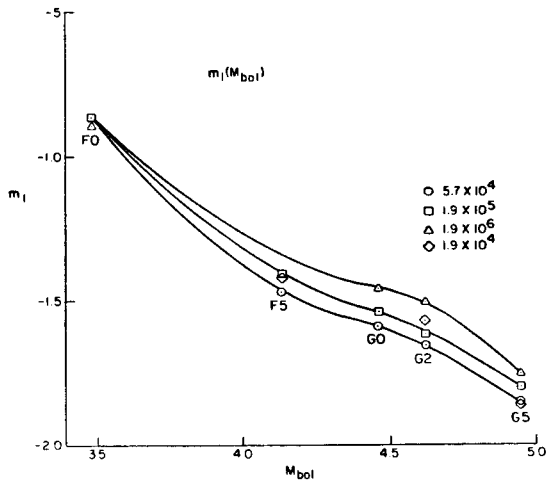

FIG. 8.—The metal index, m_1, as a function of M_{bol} with lines of constant A

The metal index is very sensitive to the model as demonstrated by Figure 8. The models for the normal abundance are not represented by a line of constant A, because m_1 decreases (toward a more negative value) from $A = 1.9 \times 10^4$ to 5.7×10^4, implying that the models with $\frac{1}{3}$ the normal abundance of metals have more metals than the normal models. The cause of this is that the strong lines, being somewhat saturated, are altered only slightly by decreasing the metal abundance. Since the pressure increases with A, the lines may show some pressure broadening offsetting or overcoming the slight drop in equivalent width caused by slightly decreased absorption. On the other hand, weak lines should begin to disappear. It is these weak lines that are not accounted for in the criterion of Section III. Comparison of Figure 1 with the Utrecht *Atlas* (Minnaert, Mulders, and Houtgast 1940) shows that this criterion has left out quite a few lines! The lines omitted by this criterion are probably insignificant in the extreme subdwarfs, so the values of m_1 are nearer reality than those of the normal stars. The data for A =

5.7×10^4, 1.9×10^5, and 1.9×10^6 are presented in Figure 8 as a function of $M_{bol} = 4.62 - \log (L/L\odot)$, assuming all the models to have solar radii. The points for the K0 models have been deleted because of their erratic behavior in m_1 and in the variation of temperature, etc., with A. The point for F5, $A = 1.9 \times 10^6$, has also been deleted because of its large $b - y$ excess. The behavior of m_1 $(b - y)$ (Figure 9) is similar to the observed plot (Strömgren 1963). Because of the lack of good theoretical values of m_1 for stars of normal abundance, these numbers cannot be used to calibrate the observations. Strömgren and Perry (1964) have metal index observations for HD140283 and HD19445. Aller and Greenstein (1960) have abundance determinations for these stars (see also Wallerstein 1962). Calibrating the G2 models by HD 19445 and the G5 models by HD 140283, it is found by least squares that $\Delta m = 0^m0881 \log (A/A\odot) + 0^m0122$. The quantity Δm is the relative metal index such that larger positive values correspond to smaller metal abundances. This agrees well with the complete comparison of data by Wallerstein (1962) and Strömgren and Perry (1964) as discussed by Strömgren (1963),

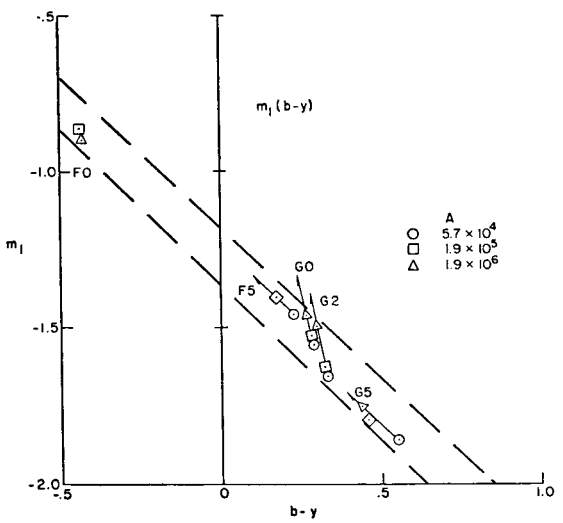

FIG. 9.—The metal index, m_1, as a function of $b-y$, grouped according to spectral type. See text

who finds that $\Delta m = 0^m083 \log (A/A\odot)$. (It has been assumed in the above that $\log [N_H/N_{Fe}]_* - \log [N_H/N_{Fe}]\odot = \log [A/A\odot]$.) Baschek (1960) obtains $\Delta m = 0.05 \log (A/A\odot)$ for G2 models only by a curve-of-growth method. This apparently good agreement with Strömgren must be viewed cautiously because the expectation of the variance yields an expected deviation of $\pm 0^m039$. However, the general trend of the model calculations agrees well with the above empirical calibration by Strömgren.

Work is in progress to overcome the problem of constancy of flux, including convection, and blanketing in order to calculate m_1 for the normal stars.

I wish to express my grateful appreciation to the following: Dr. Bengt Strömgren, Dr. T. L. Swihart, Dr. David Crawford, and Mr. Charles Perry. I would like to thank the Los Alamos Scientific Laboratory, the Indiana University Research Computing Center, and the National Aeronautics and Space Administration for computer support. My appreciation is especially extended to Dr. Marshal H. Wrubel for his advice and discussions. Part of the cost of calculation was supported by a grant to Dr. Wrubel from the National Science Foundation.

APPENDIX

In the following, we work in frequency units because the equations take a simpler form in that scheme, but we designate the point by its wavelength since this presents a clearer picture to the reader.

The expression used for the absorption due to the many weak lines is a semiempirical relation derived by Swihart (1959)

$$K_\nu(M) = \begin{cases} C_m \dfrac{X}{A} \lambda' P_e e^{28.54\theta/\lambda'} & (\lambda' < 8.0)\ , \\ 0 & (\lambda' \geq 8.0)\ , \end{cases} \tag{13}$$

where λ' is the wavelength in units of 10^3 Å, $\theta = 5040/T$, and $C_m = 0.075$.

The effect of the discernible absorption lines depends upon the number of observed lines in a wavelength region and some measure of their strength. We calculate a mean line-absorption coefficient profile, average it over the wavelength region (Table 2) under consideration,

TABLE 2

Region	λ_c'*	$\Delta\nu_R$ (sec^{-1})
I	3.45	6.0×10^{14}
II	4.15	2.31×10^{14}
III	4.65	1.77×10^{14}
IV	5.25	
V	5.85	1.51×10^{14}
VI	6.6	
VII	7.55	1.13×10^{14}
VIII	8.65	
IX	11.5	7.00×10^{13}

* λ_c' is the central wavelength of the region. Regions connected by one $\Delta\nu_R$ are taken as one region with the tabulated $\Delta\nu_R$, and a mean of their contributions is taken as described in the text.

and add it to the above-mentioned sources of continuous opacity. We begin by defining the mass absorption coefficient for a line of an element of atomic number A and atomic mass M_A,

$$l_\nu = a_\nu \frac{N_{r,i}}{\rho} \left(\frac{cm^2}{gm}\right), \tag{14}$$

where a_ν is the atomic absorption coefficient and is given by

$$a_\nu = \frac{e^2\sqrt{\pi}}{m_e c} f \frac{1}{\Delta\nu_D} H(a, v): \tag{15}$$

f is the oscillator strength;

$$\Delta\nu_D = \frac{1}{\lambda}\left(\frac{2kT}{M_A}\right)^{1/2} \tag{16}$$

is the Doppler width in frequency units; $H(a, v)$ is the well-known line-broadening function;

$N_{r,\,l}$ is the number of atoms per unit volume in the rth stage of ionization lth level of excitation; and ρ is the gas density. Writing

$$N_{r,\,l} = \frac{N_{r,\,l}}{N}\, N\,, \tag{17}$$

we can calculate $N_{r,\,l}/N$, where N is the total number of atoms of the type under consideration, from the combined Saha-Boltzmann equation. We approximate the partition functions by $U_2 = \frac{1}{2}U_1 = \frac{1}{4}U_0$; U_r being the partition function associated with the rth degree of ionization. Equation (14) can then be written

$$l_\nu = b\,\frac{1}{\rho\Delta\nu_D}\left(\frac{N_{r,\,l}}{N}\right)H(a,\,v)\,Nf\,, \tag{18}$$

where $b = e^2\sqrt{\pi}/m_e c$, representing the absorption coefficient for one line of one atom.

We obtain the mean value of equation (18) over the wavelength interval under consideration by integrating over frequency and dividing by the frequency interval. The integration is terminated at some frequency because l_ν becomes vanishingly small at some v, say $v_{\max}$. The only term in equation (18) that depends on the point in the line is $H(a, v)$. The integration of $H(a, v)$ is approximated by

$$\int H(a,\,v)\,dv \sim 2\left[\sum_{v=0}^{v_{\max}} H(a,\,v)\,\Delta v\right]\Delta\nu_D\,, \tag{19}$$

TABLE 3

$L_{r,\,l,\,s} \times 10^{15}$

WEAK LINES*

Region	X_e				
	0.5	1.5	2.5	3.5	5.5
	Neutral Atoms				
I	44.44	14.81	33.58	6.478	0
II	8.445	4.486	11.338	3.338	0
III	0.4505	0.4654	1.055	0.6816	0
IV	0.458	0.346	0.4315	1.168	0
V	0.0319	0.0684	0.1922	0.4086	0.0108
VI	0.1434	0	0.1416	0.0586	0
VII	0.0112	0.0274	0.0619	0.2971	0.1189
VIII	0.0078	0.005	0.0823	0.0908	0.1283
IX	0.7560	0.1610	4.024	13.108	0
	Ions				
I	8.706	9.232	2.588	0.6142	0
II	18.010	9.575	0	0	0
III	0.9627	0.3137	0.0632	0	0
VIII	0	0	0.004	0.0318	0.0119

* $X_1 = 7.9$ eV; $X_2 = 17$ eV; $A_r = 26$; $M_r = 56$. Regions not tabulated have all zero entries.

TABLE 3—*Continued*

STRONG LINES, CLASS I†

Region	X_e					
	0	0.25	0.5	1.0	1.5	2.5
	Neutral Atoms					
I	11.943	0	0	0	0	0
II	1.796	0	0	0	0	0
	Ions					
II	23.512	0	0	0	0	0

† $X_1 = 5.8$ eV; $X_2 = 17$ eV; $A_r = 20$; $M_r = 40$. Regions not tabulated have all zero entries.

STRONG LINES, CLASS II‡

Region	X_e					
	0	0.25	0.5	1.0	1.5	2.5
	Neutral Atoms					
I	78.202	32.88	41.403	168.137	19.958	20.304
II	2.398	0	0.7962	2.0	26.554	3.796
	Ions					
I	13.528	3.17	3.17	13.528	7.782	4.612

‡ $X_1 = 7.9$ eV; $X_2 = 17$ eV; $A_r = 26$; $M_r = 56$.

and equation (18) becomes

$$l_\nu = b\,\frac{2}{\rho}\left(\frac{N_{r,\,i}}{N}\right)Nf\left[\frac{\Sigma H(a,\,v)}{\Delta\nu_R}\right]. \tag{20}$$

The quantity Δv is taken as unity and $\Delta\nu_R$ is the width of the wavelength region in frequency units as tabulated by Labs (1951).

Labs tabulates three classes of lines, one designated as weak and two as strong. Each class is divided into the subclasses of neutral and ionized lines, with mean ionization potentials for each class. Each subclass is further subdivided according to mean excitation potentials. For each mean excitation potential there are several strengths of lines, designated by a log (NHf) value determined from a curve of growth. H is the "thickness of the atmosphere." We assume in the following that all the lines have their line center in the center of the wavelength region.

For each log (NHf) value there is tabulated the number of lines, n_k, of that strength for that mean excitation potential, etc. We multiply and divide equation (20) by H and multiply by n_k (see Table 3). We designate the quantities which depend on the mean excitation potential by l, on the mean ionization potential by r, and class of line strength by s. Equation (20) becomes

$$l_\nu = b\frac{2}{\rho H \Delta\nu_R} n_{k,r,l,s}\left(\frac{N_{r,l}}{N}\right)_s (NHf)_{k,r,l,s}\left[\sum_v H(a,v)\right]_{r,l,s}. \tag{21}$$

We can perform the sum over k and replace

$$\sum_k n_{k,r,l,s}(NHf)_{k,r,l,s}$$

by $L_{r,l,s}$. We must account for the change in N due to changing A, so we multiply $L_{r,l,s}$ by A_s/A, $A_s = 1.9 \times 10^4$. Then, summing over-all contributions, we have

$$\langle l_\nu \rangle = b\frac{A_s}{A}\frac{2}{\rho H \Delta\nu_R}\sum_{r,l,s}\left\{\left(\frac{N_{r,l}}{N}\right)_s L_{r,l,s}\left[\sum_v H(a,v)\right]_{r,l,s}\right\}, \tag{22}$$

which is added to all the above-mentioned sources of continuous opacity in order to determine the temperature-pressure relations of the models.

REFERENCES

Allen, C. W. 1955, *Astrophysical Quantities* (London: Athlone Press).
Aller, L. H. 1961, *The Abundance of the Elements* (New York: Interscience).
Aller, L. H., and Greenstein, J. 1960, *Ap. J. Suppl.*, **5**, 139.
Baschek, B. 1959, *Zs. f. Ap.*, **48**, 95.
———. 1960, *ibid.*, **50**, 296.
Chandrasekhar, S., and Breen, F. S. 1945, *Ap. J.*, **104**, 430.
Claas, W. J. 1951, *Rech. Astr. Obs. Utrecht*, **12**, 14.
Code, A. D. 1959, *Ap. J.*, **130**, 473.
Corliss, C. H., Meggers, W. F., and Bozman, W. R. 1962, *NBS Mono.*, No. 53 (Washington, D.C.: Government Printing Office).
Fischel, D. 1963, thesis, Indiana University.
Geltman, S. 1962, *Ap. J.*, **136**, 935.
Goldberg, L., Müller, E. A., and Aller, L. H. 1960, *Ap. J. Suppl.*, **5**, 1.
Griem, H. 1960, *Ap. J.*, **132**, 883.
Johnson, F. S. 1950, *J. Meteorol.*, **11**, 431.
Jurgens, G. 1954, *Zs. f. Phys.*, **138**, 613.
Kingsbury, R. F. 1955, *Phys. Rev.*, **99**, 1846.
Labs, D. 1951, *Zs. f. Ap.*, **29**, 199.
Melbourne, W. G. 1960, *Ap. J.*, **132**, 101.
Minnaert, M., Mulders, G. F. W., and Houtgast, J. 1940, *Photometric Atlas of the Solar Spectrum* (Amsterdam: Schnabel).
Moore, C. H. 1945, *Princeton Obs. Contrib. 20.*
Ohmura, T., and Ohmura, H. 1961, *Phys. Rev.*, **121**, 513.
Ornstein, L. S., and Key, J. 1934, *Physica*, **1**, 445.
Przybylski, A. 1961, *Acta Astr.*, **11**, 59.
Strömgren, B. 1940, *Festschrift f. Elis Strömgren* (Copenhagen: Munksgaard).
———. 1958, *Stellar Populations*, ed. D. J. K. O'Connell, S.J. (New York: Interscience).
———. 1963, *Quart. J.R.A.S.*, **4**, 7.
Strömgren, B., and Perry, C. 1964, private communication.
Swihart, T. L. 1956, *Ap. J.*, **123**, 139.
———. 1959, private communication.
Swihart, T., and Fischel, D. 1961, *Ap. J. Suppl.*, **5**, 291.
Vitense, E. 1953, *Zs. f. Ap.*, **32**, 135.
Wallerstein, G. 1962, *Ap. J. Suppl.*, **6**, 407.
Wallerstein, G., and Carlson, M. 1960, *Ap. J.*, **132**, 276.
Wildey, R. L., Burbidge, E. M., Sandage, A. R., and Burbidge, G. R. 1962, *Ap. J.*, **135**, 94.
Wrubel, M. H. 1962, private communication.